

Crystal Phases of Charged Interlayer Excitons in van der Waals Heterostructures

Igor V. Bondarev,^{1,*} Oleg L. Berman,^{2,3} Roman Ya. Kezerashvili,^{2,3} and Yurii E. Lozovik^{4,5}

¹*Department of Mathematics & Physics, North Carolina Central University, Durham, NC 27707, USA*

²*Physics Department, New York City College of Technology, City University of New York, NY 11201, USA*

³*Graduate School and University Center, City University of New York, NY 10016, USA*

⁴*Institute of Spectroscopy, Russian Academy of Sciences, 142190 Troitsk, Moscow Region, Russia*

⁵*National Research University "Higher School of Economics",
Tikhonov Moscow Institute of Electronics & Mathematics, 123458 Moscow, Russia*

We analyze the collective properties of charged interlayer excitons observed recently in bilayer semiconductor van der Waals heterostructures. We predict new strongly correlated phases — crystal and Wigner crystal — that can be selectively realized with bilayers of proper electron-hole effective masses and interlayer separation distance. Our results open up new avenues for nonlinear coherent control, charge transport and spinoptronics applications with van der Waals heterostructures.

Strongly correlated coherent states of excitons have been a subject of intense theoretical and experimental studies over the last decades [1–10]. The topic has gained momentum recently due to new emerging materials of reduced dimensionality such as atomically thin van der Waals (vdW) bound layers of semiconducting transition metal dichalcogenides (TMDs) [11–18]. These layered quasi-two-dimensional (2D) semiconductors make the exciton formation possible of electrons and holes located in distinct layers [19–24]. Due to the dimensionality reduction and because of a greatly reduced electron-hole wavefunction overlap, interlayer (or indirect) excitons thus formed have large binding energies and long lifetimes. Being electrically neutral, they feature a permanent electric dipole moment directed perpendicular to the layers, offering tunability of their quantum states by an external electric field. Similar to indirect excitons in conventional GaAs based coupled quantum well systems [25, 26], the interlayer excitons (IE) in vdW heterostructures can be coupled to light to form dipolar exciton-polaritons, allowing control of quantum phenomena such as electromagnetically induced transparency, adiabatic photon-to-electron transfer, room-temperature Bose-Einstein condensation (BEC) and superconductivity [27–32].

For bilayer TMD heterostructures, controlled optical and electrical generation of IEs and *charged* IEs (CIEs, also known as trions formed by indirect excitons [33]) has lately been achieved [23, 24]. Their in-plane propagation through the sample was adjusted by the excitation power and perpendicular electrostatic field. These experiments exhibit a unique potential of TMD bilayers for achieving precise control over composite quantum particles of both bosonic (IE) and fermionic (CIE) nature. The CIEs offer even more flexibility in this respect as they have both net charge and permanent dipole moment as well as non-zero spin (Fig. 1), to allow for electrical tunability and optical spin manipulation in charge transport and spinoptronics experiments with quasi-2D vdW heterostructures.

Here, we consider the collective properties of the negative and positive CIEs starting with their binding ener-

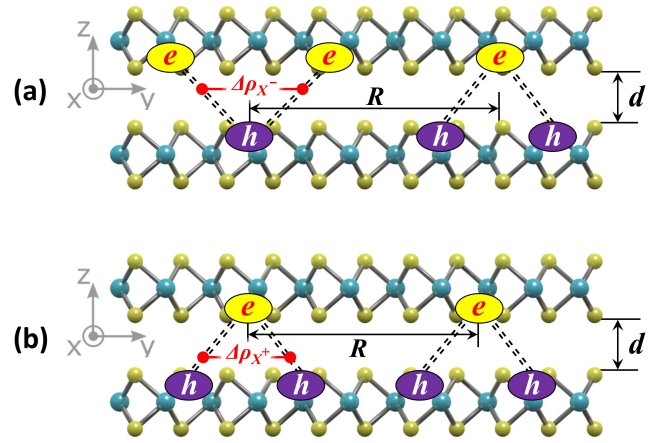


FIG. 1. (Color online) The composite structure and pairwise interaction geometry for the unlike-charge (a) and like-charge (b) interlayer exciton complexes (trions) in a bilayer quasi-2D semiconductor.

gies in bilayer quasi-2D semiconductor heterostructures. We derive the general analytical expressions as functions of the electron-hole effective mass ratio and interlayer separation distance to explain the experimental evidence earlier reported for the negative CIE to have a greater binding energy than that of the positive CIE [23]. Our analysis of the pairwise interactions between the CIEs, as sketched in Fig. 1, exhibits two scenarios for crystallization phase transitions in the collective multiparticle CIE system. They are the crystallization of the unlike-charge CIEs and the Wigner crystallization of the like-charge CIEs, which can be selectively realized in practice by choosing bilayers with appropriate electron-hole effective mass ratio and interlayer separation in addition to the standard technique of electrostatic doping. We conclude that this strongly correlated multiexciton phenomenon of CIE crystallization can be realized in layered van der Waals heterostructures such as double bilayer graphene and bilayer TMD systems [23, 31], to open up new avenues for nonlinear coherent optical control and spinoptronics applications with charged interlayer excitons.

* Corresponding author email: ibondarev@nccu.edu

The binding energy.— The composite structure of the CIE complexes of interest is sketched in Fig. 1. We use the configuration space approach [34] to derive the binding energy expressions for the CIEs as functions of their electron-hole effective mass ratio $\sigma = m_e/m_h$ and interlayer separation distance d . This approach was recently proven to be efficient as applied to quasi-1D [35] and quasi-2D bilayer semiconductors [33] where it offers easily tractable analytical solutions to reveal universal relations between the binding energy of the complex of interest and that of the 1D-exciton or that of the indirect (interlayer) exciton [36], respectively. The method itself was originally pioneered by Landau [37], Gor'kov and Pitaevski [38], Holstein and Herring [39] in their studies of molecular binding and magnetism.

The negative X^- (positive X^+) trion complex in Fig. 1 can be viewed as two equivalent IEs sharing the same hole (electron). The CIE bound state then forms due to the exchange under-barrier tunneling between the *equivalent* configurations of the electron-hole system in the configuration space of the *two independent* relative electron-hole motion coordinates representing the two equivalent IEs that are separated by the center-of-mass-to-center-of-mass distance $\Delta\rho$. The binding strength is controlled by the exchange tunneling rate integral $J_{X\pm}(\Delta\rho)$. The CIE binding energy is

$$E_{X\pm}(\sigma, d) = -J_{X\pm}(\Delta\rho = \Delta\rho_{X\pm}) \quad (1)$$

with $\Delta\rho_{X\pm}$ to be determined from an appropriate variational procedure to maximize the tunneling rate, which corresponds to the CIE ground state. This approach gives an upper bound for the (negative) *ground* state binding energy of an exciton complex of interest [33–35]. It captures essential kinematics of the formation of the complex and helps understand the general physical principles to underlie its stability.

Using the configuration space method for solving the CIE ground state binding energy problem, we obtain [40]

$$J_{X\pm}(\Delta\rho) = 2N^4\Delta\rho^2 \exp\left[-2\alpha\left(\sqrt{\Delta\rho^2 + 4d^2} - 2d\right)\right] \times \left[\frac{\alpha}{\sqrt{\Delta\rho^2 + 4d^2}} + \frac{1}{2\left(r_0 + \left\{\frac{1}{\sigma}\right\}\Delta\rho/\lambda\right)(\alpha\Delta\rho - 1)} \right] \frac{\lambda\Delta\rho}{\left(\frac{r_0 + \left\{\frac{1}{\sigma}\right\}\Delta\rho/\lambda}{r_0 + \Delta\rho}\right)\left\{\frac{\sigma}{1}\right\}(\alpha\Delta\rho - 1)}, \quad (2)$$

where $\alpha = 2/(1+2\sqrt{d})$ and $N = 4/\sqrt{1+4\sqrt{d}+8d(1+\sqrt{d})}$ are the interlayer separation dependent constants coming from the indirect (interlayer) exciton wave function [36], and the upper or lower term should be taken in the curly brackets for the positive or negative CIE, respectively. Here the 3D "atomic units" are used [36–39], with distance and energy measured in the units of exciton Bohr radius $a_B^* = 0.529 \text{ \AA} \varepsilon/\mu$ and exciton Rydberg energy

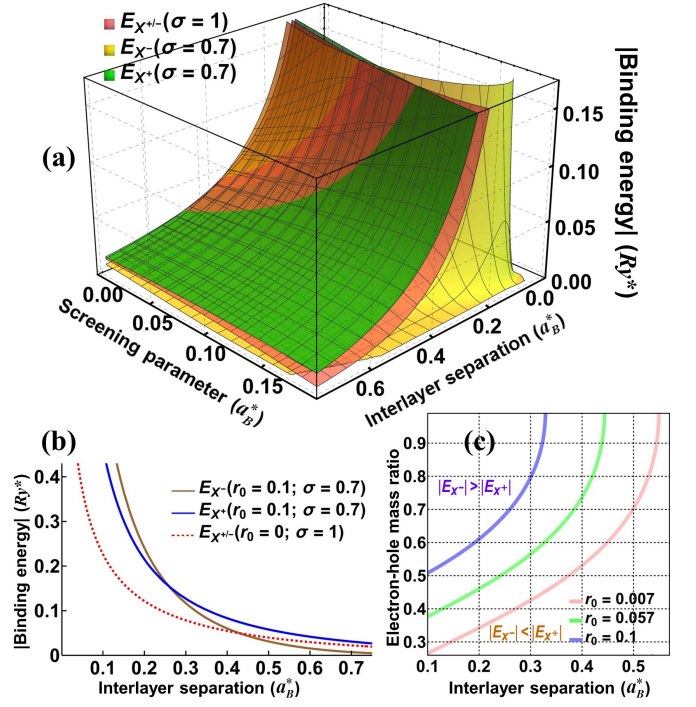


FIG. 2. (Color online) (a) Binding energies of the positive and negative CIEs as functions of the interlayer separation d and screening length r_0 as given for $\sigma=1$ and 0.7 by Eqs. (1), (2) and (4). (b) Crosscuts of (a) for $r_0=0$ and 0.1 to show the binding energy splitting for the positive and negative CIEs with unequal electron-hole masses. (c) Solutions to equation $E_{X^+}(\sigma, d) = E_{X^-}(\sigma, d)$ for three values of the screening length.

$Ry^* = \hbar^2/(2\mu m_0 a_B^{*2}) = e^2/(2\varepsilon a_B^*) = 13.6 \text{ eV } \mu/\varepsilon^2$, respectively, ε represents the *effective* average dielectric constant of the bilayer heterostructure and $\mu = m_e/(\lambda m_0)$ stands for the exciton reduced effective mass (in the units of free electron mass m_0) with $\lambda = 1 + m_e/m_h = 1 + \sigma$. The image-charge effects are neglected [36]. To properly take into account the screening effect for the charges forming the CIEs as sketched in Fig. 1, we used the Keldysh-Rytova interaction potential (see Ref. [41]) approximated by elementary functions in the form

$$V_{\text{eff}}(\rho) = \frac{1}{r_0} \left[\ln\left(1 + \frac{r_0}{\rho}\right) + (\ln 2 - \gamma)e^{-\rho/r_0} \right] \quad (3)$$

proposed for atomically thin layers in Ref. [42], to represent the effective electrostatic potential for like charges in monolayers. Here, ρ is the in-plane intercharge distance and $r_0 = 2\pi\chi_{2D}$ is the screening length parameter with χ_{2D} being the in-plane polarizability of 2D material [42, 43]. For unlike charges the interlayer electrostatic potential is taken to be in the standard Coulomb form $V_C(r) = -1/r$ with $r = \sqrt{\rho^2 + d^2}$.

The function $J_{X\pm}(\Delta\rho)$ in Eq. (2) is clearly seen to have a maximum. It tends to become a negative when $\alpha\Delta\rho < 1$ in the second term in the square brackets, which is always the case for large enough d whereby $\alpha \approx 1/\sqrt{d} \sim 0$ and the first term in the square brackets is

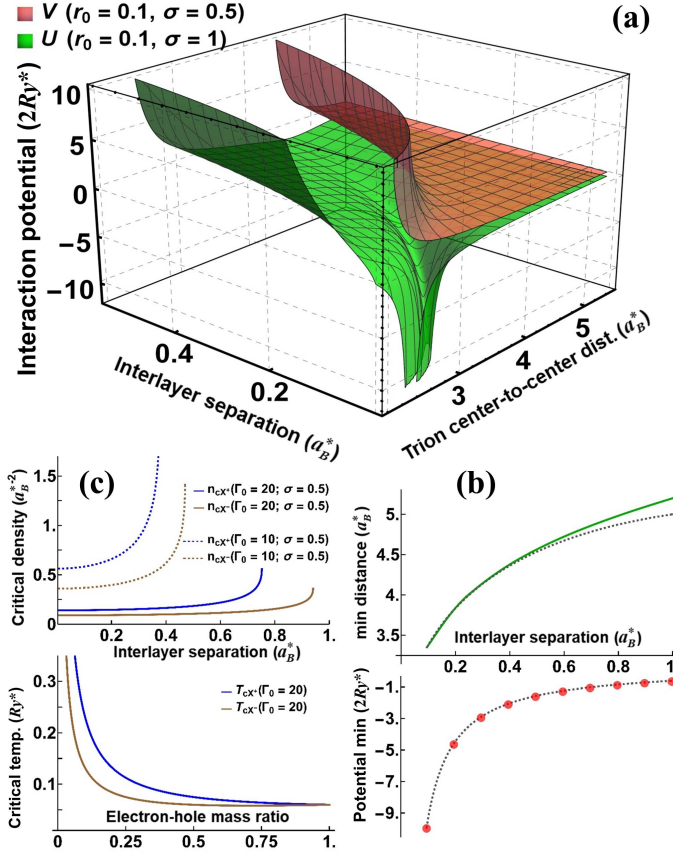


FIG. 3. (Color online) (a) The exact electrostatic interaction potentials U (attractive) and V (repulsive) as functions of R and d calculated for the pairs of unlike- and like-charge trions with $\sigma = 1$ and 0.5 , respectively, in their symmetry-promoted most likely configurations shown in Fig. 1. (b) The approximate analytical (dashed black lines) and calculated d_{\min} (top, green line) and U_{\min} (bottom, red dots) for the U -potential surface in (a). (c) Critical densities (top) and temperatures (bottom) for the Wigner crystallization transition of the manyparticle system of like-charge trions.

negligible, whereas for $\alpha\Delta\rho > 1$ it is manifestly positive and approaching zero as $\Delta\rho$ increases. Extremum seeking under the condition that $\Delta\rho > 1$ to *only* include the leading terms in small $1/\Delta\rho$, gives a compact result [40]

$$\Delta\rho_{X^\pm} = \frac{7\alpha - 1 - \left\{\frac{\sigma}{1/\sigma}\right\}}{2\alpha^2} - \left(3 + 2\left\{\frac{\sigma}{1/\sigma}\right\}\right)r_0. \quad (4)$$

Substituting this in Eq. (1), one obtains the positive and negative CIE binding energies of interest.

Figure 2 (a) shows the binding energies E_{X^+} and E_{X^-} calculated from Eqs. (1), (2) and (4) with $\sigma = 1$ and 0.7 as functions of d and r_0 . For $\sigma = 1$ they coincide [33]. For $\sigma = 0.7$ the positive-negative CIE binding energy splitting is seen to occur in the entire domain of parameters used. Figure 2 (b) shows the crosscuts of Fig. 2 (a) for $r_0 = 0$ and 0.1 to exhibit the remarkable features of the screening and binding energy splitting effects. The screening

of like charges in the CIE complex is seen to increase its binding energy. The X^\pm trion energy splitting at short d is such that $|E_{X^-}| > |E_{X^+}|$, which agrees with and thus explains the measurements reported recently for (h-BN)-encapsulated MoSe₂-WSe₂ bilayer heterostructures [23]. As d increases the crossover occurs to give $|E_{X^-}| < |E_{X^+}|$ with $|E_{X^-}|$ quickly going down to zero, which is also seen in Fig. 2 (a). On closer inspection of Eqs. (2) and (4) it can be seen though that $|E_{X^-}|$ and $|E_{X^+}|$ swap places for $\sigma > 1$ (not shown here), thereby offering an extra functionality for properly fabricated vdW heterostructures.

Equation $E_{X^+}(\sigma, d) = E_{X^-}(\sigma, d)$ links the electron-hole mass ratio σ and interlayer separation d at which the crossover occurs. For $\sigma = 1$ it turns into an identity [33]. The three lines in Fig. 2 (c) present the nontrivial solution to this equation, $\sigma(d)$, for three different r_0 values. The screening is seen to shrink the $|E_{X^-}| > |E_{X^+}|$ domain and expand the $|E_{X^-}| < |E_{X^+}|$ domain (above and below the solution line, respectively). Since the greater binding energy increases the formation probability, these domains are also those to preferentially form the X^- and X^+ trion, respectively, while the constraint $E_{X^-} = E_{X^+}$ defines the line of equal X^\pm formation probabilities. Thus by varying d for a properly chosen TMD bilayer composition with known σ , one can selectively control *intrinsic* positive/negative CIE formation in an undoped heterostructure as opposed to the electrostatic doping technique.

Unlike-charge trion crystallization.— For undoped structures of two monolayers with $\sigma = 1$ as well as for those with $\sigma \neq 1$ fabricated to hit the $E_{X^-} = E_{X^+}$ line, both X^- and X^+ trions are equally likely to form under intense external irradiation at not too high temperatures $T < |E_{X^\pm}|/k_B$. This results in an overall neutral two-component manyparticle mixture of X^- and X^+ trions. The aggregate state of a manyparticle system is defined by its Helmholtz free energy consisting of the total energy term and the entropy term. The entropy term becomes dominant at high T to favor configurations with greater randomness. At not too high T the total energy term — the sum of kinetic, potential and binding energies of individual particles — overcomes the entropy term so that an ordered state is favored, with the order-disorder transition being predominantly determined by the interparticle pairwise interaction potential energy [44].

The long-range Coulomb interaction of the pair of CIEs (trions) is strengthened by their permanent dipole moments directed perpendicular to the plane of the structure to provide the stronger attraction/repulsion for the unlike/like-charge trion pairs. Their actual *exact* interaction potential depends on the relative orientation of the triangles formed by the three charges in a trion complex. The exact potential includes nine terms to couple electrons and holes in two complexes by means of the $V_{\text{eff}}(R, \Delta\rho_{X^\pm}, r_0)$ and $V_c(R, \Delta\rho_{X^\pm}, d)$ potentials, where R is the trion center-to-center distance [40]. Figure 3 (a) shows the exact interaction potentials U and V as functions of R and d for unlike- and like-charge trion pairs (shown for $\sigma = 1$ and 0.5 , respectively; no major change

observed with the variation of σ) in their symmetry-promoted most likely configurations presented in Fig. 1. The unlike-charge trion pairwise interaction potential exhibits a deep attractive (negative) minimum and a strongly repulsive (positive) core for all d in the range presented, in contrast with the manifestly repulsive like-charge trion pairwise potential. This is what makes the order-disorder transition in the two-component unlike-charge trion system identical to that in a 1D antiferromagnet, or that in an AB type alloy with A and B components randomly mixed at high T and ordered on the ionic-crystal-type superlattice of interpenetrating a - and b -sublattices below $T_c^{(N)} = zv/2k_B$, the Néel temperature [44]. Here, z is the number of the nearest neighbors on the superlattice and $v = (v_{AA} + v_{BB})/2 - v_{AB} > 0$ is the combined nearest-neighbor coupling constant written in terms of those of respective sublattices. In our case here, the ordering below $T_c^{(N)}$ creates 1D chains ($z=2$) of the two interpenetrating sublattices with collinear CIE permanent dipole moments in each of the two, which are antiparallel to each other. In full analogy, taking the parameters R_{\min} and $U_{\min} = U(R_{\min})$ of the minimum of the potential U in Fig. 3 (a) to represent the chain period and the unlike-charge trion coupling constant, respectively, one obtains $T_c^{(N)} \approx [V(2R_{\min}) - U(R_{\min})]/k_B \approx |U_{\min}|/k_B$. Here, $V(2R_{\min}) \approx 0$ stands for the repulsive interaction coupling constant of the like-charge trions whose sublattice period is twice greater than the period of the chain.

The top and bottom panels in Fig. 3 (b) present the exact d -dependences of R_{\min} and U_{\min} calculated for the U -potential surface shown in Fig. 3 (a). Their approximate expressions can be relatively easily found analytically by seeking the U -potential minimum under the conditions $r_0, d < 1$ and $\Delta\rho_{X\pm} > 1$ consistent with Eq. (4). This leads to $R_{\min} \approx (r_{ee} + r_{hh})/2$ and $U_{\min} \approx -1/d + 1/r_{ee} + 1/r_{hh}$, where $r_{ee} = (\lambda/\sigma)\Delta\rho_{X-}$ and $r_{hh} = \lambda\Delta\rho_{X+}$ are the inter-electron and interhole distances in the negative and positive CIE, respectively. These expressions are seen to reproduce the numerical calculations quite well, within the approximations used, to demonstrate the fast drop of $|U_{\min}|$ (and T_{cN} for the unlike-charge trion crystallization transition, accordingly) with R_{\min} slowly rising as the interlayer separation d in the heterostructure increases.

Like-charge trion Wigner crystallization.— In heterostructures of two monolayers with $\sigma \neq 1$ separated by an interlayer distance *not* to fulfill the $E_{X-}(\sigma, d) = E_{X+}(\sigma, d)$ constraint, including electrostatically doped heterostructures, either X^- or X^+ trions are most likely to form under intense irradiation. As can be seen from Fig. 2, for $\sigma < 1$ the domains $|E_{X-}| > |E_{X+}|$ and $|E_{X-}| < |E_{X+}|$ are located at smaller and greater d to form like-charge trions — negative and positive, respectively, as long as their binding energy absolute values exceed the thermal fluctuation energy at a given T .

An ensemble of repulsively interacting particles (or quasiparticles, structureless or composite) forms a Wigner lattice when its average potential interaction energy exceeds average kinetic energy, $\langle V \rangle / \langle K \rangle = \Gamma_0 > 1$. This

was previously shown for systems such as 2D electron gas [45], cold polar molecules [46], and indirect excitons [4]. For like-charge trions in Fig. 1 (b), the Coulomb repulsion at large R is strengthened at shorter R by the dipole-dipole repulsion of their collinear permanent dipole moments (to result in the pairwise interaction potential V illustrated in Fig. 3), while the total kinetic energy is additionally contributed by the rotational term $K_{X\pm}^{(r)} = \hbar^2 l(l+1)/2I_{X\pm}$ with $l = 0, 1, 2, \dots$ being the orbital quantum number and $I_{X\pm} = m_{h,e} r_{hh,ee}/2$ representing the moment of inertia for CIE rotation about its permanent dipole moment direction. The low- T statistical averaging over l leads to the characteristic rotational motion "freezing" temperature $T_{X\pm}^{(r)} = \hbar^2/k_B I_{X\pm}$ (see, e.g., Ref. [47]). By direct analogy with the hydrogen molecular ion problem this can be rewritten as $T_{X+}^{(r)} \approx \sigma |E_{X+}|/k_B$ and $T_{X-}^{(r)} \approx |E_{X-}|/k_B \sigma$ (see, e.g. Ref. [48]), indicating the rotational degrees of freedom to be frozen out (at least for the case of σ being close to unity typical of TMDs, in particular [49, 50]) as long as the CIEs are stable against the thermal fluctuations.

With no rotational term contribution, it is straightforward to get a qualitative picture of the like-charge trion Wigner crystallization by performing an analysis analogous to that done in Ref. [45] for the 2D electron gas. With slight modifications to include the dipole repulsion in the interparticle interaction potential V and to replace the electron mass by the CIE mass in the translational kinetic energy K , the expressions for the zero- T critical density n_c and for the critical temperature $T_c^{(w)}$ of the Wigner crystallization phase transition take the form [40]

$$n_{cX\pm} = \frac{2}{\pi d^2} \left(\frac{g_{\pm} \Gamma_0}{4d} \right)^2 \left[1 - \frac{1}{2} \left(\frac{4d}{g_{\pm} \Gamma_0} \right)^2 - \sqrt{1 - \left(\frac{4d}{g_{\pm} \Gamma_0} \right)^2} \right],$$

$$k_B T_{cX\pm}^{(w)} = \frac{4Ry^*}{g_{\pm} \Gamma_0^2}, \quad (5)$$

$$g_{\pm}(\sigma) = \left(3 + \left\{ \frac{1}{2} \right\} \sigma + \left\{ \frac{2}{1} \right\} \frac{1}{\sigma} \right)^{-1}.$$

The quantities $n_{cX\pm}$ and $T_{cX\pm}^{(w)}$ are shown on the top and bottom of Fig. 3 (c) as functions of d and $\sigma (< 1)$, respectively, for moderate Γ_0 values [45]. As d increases so does $\langle V \rangle$ once the dipole repulsion becomes appreciable. With constant Γ_0 this leads to the $\langle K \rangle$ increase and $n_{cX\pm}$ rise, accordingly. The latter is slightly lower for the negative CIE due to its smaller K because of the smaller mass than that of the positive CIE. Lowering σ generally lowers the CIE mass thus decreasing its K whereby $T_{cX\pm}^{(w)}$ increases. These are the general trends featured in Fig 3 (c).

Estimates for the effects discussed.— In our model only two parameters are needed, ε and μ , to evaluate the effects predicted. We choose nominal $\varepsilon = 14$ and $\mu = 0.25$ typical of TMDs [43] to get $a_B^* \approx 30$ Å and $Ry^* \approx 0.02$ eV. Then $d = 0.2$ corresponds to the vdW interlayer distance of 0.6 nm earlier reported experimentally [23]. This gives $T_c^{(N)} \approx 850$ K, $T_{cX\pm}^{(w)} \approx 20$ K and $n_{cX\pm} \approx 10^{12} \text{ cm}^{-2}$ as per

graphs in Fig. 3 (b) and (c). The fact of $T_c^{(w)}$ being much greater than $|E_{X\pm}|/k_B$ (typically ~ 10 meV [23, 33]) tells that the "antiferromagnetically" ordered 1D chain phase is the actual ground state of the manyparticle like-charge trion system. The obtained $n_{cX\pm}$ and $T_{cX\pm}^{(w)}$ are, respectively, close to and exceed those reported experimentally for IEs [23, 31]. This suggests that the Wigner crystallized CIE phase can be realized in properly fabricated vdW heterostructures with the twofold overbalance of negative [as in Fig. 1 (b)] or positive charge carriers.

To summarize, we predict the existence of new strongly correlated collective CIE states in highly excited vdW heterostructures such as bilayer TMD and double bilayer graphene systems. These states represent the long-range ordered phases of the excited system — the crystal phase

and the Wigner crystal phase. A relevant analysis of the photoemission properties of crystallized excitonic states can be found in Ref. [9]. We evaluate the critical temperatures and density for the formation of such manyparticle collective crystallized CIE states. We demonstrate that they can be selectively realized with bilayers of properly chosen electron-hole effective mass ratio by just varying their interlayer separation distance. We believe that these results open up new avenues for nonlinear coherent control, charge transport and spinoptronics applications with van der Waals heterostructures.

Acknowledgments. — This research is supported by the U.S. Department of Energy, Office of Science, Office of BES under award No. DE-SC0007117 (I.V.B.), by the U.S. ARO grant No. W911NF1810433 (O.L.B., R.Y.K.), and by the RFBR grant No. 20-02-00410 (Y.E.L.).

-
- [1] L.V.Keldysh and A.N.Kozlov, Collective properties of excitons in semiconductors, *Phys. JETP* **27**, 521 (1968).
 - [2] Yu.E.Loikov and V.I.Yudson, A new mechanism for superconductivity: pairing between spatially separated electrons and holes, *Sov. Phys. JETP* **44**, 389 (1976).
 - [3] T.Fukuzawa, S.Kano, T.Gustafson, and T.Ogawa, Possibility of coherent light emission from Bose condensed states of SEHPs, *Surf. Sci.* **228**, 482 (1990).
 - [4] G.E.Astrakharchik, J.Boronat, I.L.Kurbakov, and Yu.E.Loikov, Quantum phase transition in a two-dimensional system of dipoles, *Phys. Rev. Lett.* **98**, 060405 (2007).
 - [5] O.L.Berman, Yu.E.Loikov, and G.Gumbs, Bose-Einstein condensation and superfluidity of magnetoexcitons in bilayer graphene, *Phys. Rev. B* **77**, 155433 (2008).
 - [6] G.J.Schinner, J.Repp, E.Schubert, A.K.Rai, D.Reuter, A.D.Wieck, A.O.Govorov, A.W.Holleitner, and J.P.Kotthaus, Confinement and interaction of single indirect excitons in a voltage-controlled trap formed inside double InGaAs quantum wells, *Phys. Rev. Lett.* **110**, 127403 (2013).
 - [7] O.L.Berman, R.Ya.Kezerashvili, and S.M.Tsiklauri, Triions in coupled quantum wells and Wigner crystallization, *J. Mod. Phys. B* **28**, 1450064 (2014).
 - [8] M.M.Fogler, L.V.Butov, and K.S.Novoselov, High- T superfluidity with indirect excitons in van der Waals heterostructures, *Nature Commun.* **5**, 4555 (2014).
 - [9] R.A.Suris, Gas-crystal phase transition in a 2D dipolar exciton system, *JETP* **122**, 602 (2016).
 - [10] M.Kremser, M.Brotons-Gisbert, J.Knörzer, J.Gückelhorn, M.Meyer, M.Barbone, A.V.Stier, B.D.Gerardot, K.Müller, and J.J.Finley, Discrete interactions between a few interlayer excitons trapped at a MoSe₂-WSe₂ heterointerface, E-print arXiv:1907.08815
 - [11] K.F.Mak and J.Shan, Photonics and optoelectronics of 2D semiconductor transition metal dichalcogenides, *Nature Photon.* **10**, 216 (2016).
 - [12] Y.Sun, R.Wang, and K.Liu, Substrate induced changes in atomically thin 2-dimensional semiconductors: Fundamentals, engineering, and applications, *Appl. Phys. Rev.* **4**, 011301 (2017).
 - [13] G.Wang, A.Chernikov, M.M.Glazov, T.F.Heinz, X.Marie, T.Amand, and B.Urbaszek, Colloquium: Excitons in atomically thin transition metal dichalcogenides, *Rev. Mod. Phys.* **90**, 021001 (2018).
 - [14] O.Witham, R.J.Hunt, and N.D.Drummond, Stability of triions in coupled quantum wells modeled by two-dimensional bilayers, *Phys. Rev. B* **97**, 075424 (2018).
 - [15] T.Deilmann and K.S.Thygesen, Interlayer triions in the MoS₂/WS₂ van der Waals Heterostructure, *Nano Lett.* **18**, 1460 (2018).
 - [16] Y.E.Loikov, New effects in and the control of the exciton system in quasi-two-dimensional structures, *Physics–Uspekhi* **61**, 1094 (2018).
 - [17] R.Ya.Kezerashvili, Few-body systems in condensed matter physics, *Few-Body Syst.* **60**, 52 (2019).
 - [18] M.Sammon and B.I.Shklovskii, Attraction of indirect excitons in van der Waals heterostructures with three semiconducting layers, *Phys. Rev. B* **99**, 165403 (2019).
 - [19] P.Rivera, J.Schaibley, A.M.Jones, J.S.Ross, S.Wu, G.Aivazian, P.Klement, K.Seyler, G.Clark, N.J.Ghimire, J.Yan, D.G.Mandrus, W.Yao, and X.Xu, Observation of long-lived interlayer excitons in monolayer MoSe₂-WSe₂ heterostructures, *Nature Commun.* **6**, 6242 (2015).
 - [20] J.S.Ross, P.Rivera, J.Schaibley, E.Lee-Wong, H.Yu, T.Taniguchi, K.Watanabe, J.Yan, D.Mandrus, D.Cobden, W.Yao, and X.Xu, Interlayer exciton optoelectronics in a 2D heterostructure p - n junction, *Nano Lett.* **17**, 638 (2017).
 - [21] M.Baranowski, A.Sorrente, L.Klopotowski, J.M.Urban, N.Zhang, D.K.Maude, K.Wiatowski, S.Mackowski, Y.C.Kung, D.Dumcenco, A.Kis, and P.Plochocka, Probing the interlayer exciton physics in a MoS₂/MoSe₂/MoS₂ van der Waals heterostructure, *Nano Lett.* **17**, 6360 (2017).
 - [22] B.Miller, A.Steinhoff, B.Pano, J.Klein, F.Jahnke, A.Holleitner, and U.Wurstbauer, Long-lived direct and indirect interlayer excitons in van der Waals heterostructures, *Nano Lett.* **17**, 5229 (2017).
 - [23] L.A.Jauregui, A.Y.Joe, K.Pistunova, D.S.Wild, A.A.High, Y.Zhou, G.Scuri, K.De Greve, A.Sushko, C.-H.Yu, T.Taniguchi, K.Watanabe, D.J.Needleman, M.D.Lukin, H.Park, and P.Kim, Electrical control of interlayer exciton dynamics in atomically thin heterostructures, *Science* **366**, 870 (2019).

- [24] E.V.Calman, L.H.Fowler-Gerace, D.J.Choksy, L.V.Butov, D.E.Nikonov, I.A.Young, S.Hu, A.Mishchenko, and A.K.Geim, Indirect excitons and trions in $\text{MoSe}_2/\text{WSe}_2$ van der Waals heterostructures, *Nano Lett.* **20**, 1869 (2020).
- [25] D.W.Snoke, Dipole excitons in coupled quantum wells: Towards an equilibrium exciton condensate, in: *Quantum Gases: Finite Temperature and Non-equilibrium Dynamics*, eds. N.Proukakis, S.Gardiner, M.Davis, and M.Szymańska (Imperial College, London, 2013), p. 419.
- [26] L.V.Butov, Collective phenomena in cold indirect excitons, *JETP* **122**, 434 (2016).
- [27] P.Cristofolini, G.Christmann, S.I.Tsintzos, G.Deligeorgis, G.Konstantinidis, Z.Hatzopoulos, P.G.Savvidis, and J.J.Baumberg, Coupling quantum tunneling with cavity photons, *Science* **336**, 704 (2012).
- [28] M.H.Szymanska, Intertwining electron tunneling with light, *Science* **336**, 679 (2012).
- [29] O.Cotlet, S.Zeytinoglu, M.Sigrist, E.Demler, and A.Imamoğlu, Superconductivity and other collective phenomena in a hybrid Bose-Fermi mixture formed by a polariton condensate and an electron system in two dimensions, *Phys. Rev. B* **93**, 054510 (2016).
- [30] A.Kavokin and P.Lagoudakis, Exciton-mediated superconductivity, *Nature Mater.* **15**, 599 (2016).
- [31] J.I.A.Li, T.Taniguchi, K.Watanabe, J.Hone, and C.R.Dean, Excitonic superfluid phase in double bilayer graphene, *Nature Phys.* **13**, 751 (2017).
- [32] Z.Sun, J.Beaumariage, Q.Cao, K.Watanabe, T.Taniguchi, B.Hunt, I.V.Bondarev, and D.W.Snoke, Toward a room temperature Schafroth superconductor based on charged excitonic complexes, E-print arXiv:2003.05850
- [33] I.V.Bondarev and M.R.Vladimirova, Complexes of dipolar excitons in layered quasi-two-dimensional nanostructures, *Phys. Rev. B* **97**, 165419 (2018).
- [34] I.V.Bondarev, Configuration space method for calculating binding energies of exciton complexes in quasi-1D/2D semiconductors, *Mod. Phys. Lett. B* **30**, 1630006 (2016).
- [35] I.V.Bondarev, Asymptotic exchange coupling of quasi-1D excitons in carbon nanotubes, *Phys. Rev. B* **83**, 153409 (2011); Relative stability of excitonic complexes in quasi-1D semiconductors, *ibid.* **90**, 245430 (2014).
- [36] R.P.Leavitt and J.W.Little, Simple method for calculating exciton binding energies in quantum-confined semiconductor structures, *Phys. Rev. B* **42**, 11774 (1990).
- [37] L.D.Landau and E.M.Lifshitz, *Quantum Mechanics. Non-Relativistic Theory* (Pergamon, Oxford, 1991)
- [38] L.P.Gor'kov and L.P.Pitaevski, The splitting energy of hydrogen molecule therms, *Dokl. Akad. Nauk SSSR* **151**, 822 (1963) [English transl.: *Soviet Phys.—Dokl.* **8**, 788 (1964)].
- [39] C.Herring, Critique of the Heitler-London method of calculating spin couplings at large distances, *Rev. Mod. Phys.* **34**, 631 (1962); C.Herring and M.Flicker, Asymptotic exchange coupling of two hydrogen atoms, *Phys. Rev.* **134**, A362 (1964).
- [40] See the *Supplementary Info* file included.
- [41] L.V.Keldysh, Coulomb interaction in thin semiconductor and semimetal films, *Sov. Phys. JETP* **29**, 658 (1979); N.S.Rytova, Screened potential of a point charge in a thin film, *Proc. MSU Phys., Astron.* **3**, 30 (1967).
- [42] P.Cudazzo, I.V.Tokatly, and A.Rubio, Dielectric screening in two-dimensional insulators: Implications for excitonic and impurity states in graphene, *Phys. Rev. B* **84**, 085406 (2011).
- [43] T.C.Berkelbach, M.S.Hybertsen, and D.R.Reichman, Theory of neutral and charged excitons in monolayer transition metal dichalcogenides, *Phys. Rev. B* **88**, 045318 (2013).
- [44] R.Kubo, H.Ichimura, T.Usui, and N.Hashitsume, *Statistical Mechanics. An Advanced Course with Problems as Solutions* (Elsevier, Amsterdam, 1988).
- [45] P.M.Platzman and H.Fukuyama, Phase diagram of the two-dimensional electron liquid, *Phys. Rev. B* **10**, 3150 (1974).
- [46] H.P.Büchler, E.Demler, M.Lukin, A.Micheli, N.Prokofiev, G.Pupillo, and P.Zoller, Strongly correlated 2D quantum phases with cold polar molecules: controlling the shape of the interaction potential, *Phys. Rev. Lett.* **98**, 060404 (2007).
- [47] R.K.Pathria and P.D.Beale, *Statistical Mechanics* (Elsevier, Amsterdam, 2011).
- [48] E.S.Abers, *Quantum Mechanics* (Addison-Wesley, New York, 2004), p. 237.
- [49] T.Cheiwchanchamnangij and W.R.L.Lambrecht, Quasi-particle band structure calculation of monolayer, bilayer, and bulk MoS_2 , *Phys. Rev. B* **85**, 205302 (2012).
- [50] A.Ramasubramaniam, Large excitonic effects in monolayers of molybdenum and tungsten dichalcogenides, *Phys. Rev. B* **86**, 115409 (2012).

Supplementary Information for
”Crystal Phases of Charged Interlayer Excitons
in van der Waals Heterostructures”

Igor V. Bondarev*

*Department of Mathematics & Physics,
North Carolina Central University, Durham, NC 27707, USA*

Oleg L. Berman and Roman Ya. Kezerashvili

*Physics Department, New York City College of Technology,
City University of New York, NY 11201, USA and
Graduate School and University Center,
City University of New York, NY 10016, USA*

Yurii E. Lozovik

*Institute of Spectroscopy, Russian Academy of Sciences,
142190 Troitsk, Moscow Region, Russia and
National Research University ”Higher School of Economics”,
Tikhonov Moscow Institute of Electronics & Mathematics, 123458 Moscow, Russia*

* Corresponding author email: ibondarev@nccu.edu

I. THE CHARGED INTERLAYER EXCITON BINDING ENERGY

A sketch of a charged interlayer exciton (CIE, or trion) in a TMD bilayer is presented in Fig. 1 for the negative trion case (X^-). The positive trion case (X^+) can be obtained by the charge sign inversion. The CIE we deal with here is a charged three-particle complex of an interlayer (indirect) exciton (IE) and an extra hole (h) or electron (e), in which two like charge carriers confined to the same layer share an unlike charge carrier on the other layer. Such a CIE complex can be viewed as being formed by the *two* equivalent indistinguishable symmetric IE configurations with an extra charge carrier attached to the left or right IE, respectively, as shown in Fig. 1 for the negative trion case [1]. For such a quantum system the effective configuration space can be represented by the two *independent* in-plane projections ρ_1 and ρ_2 of the relative e - h coordinates (relative to the center of mass) of each of the IEs, whereby the X^\pm ground-state Hamiltonian takes the following form [2]

$$\begin{aligned} \hat{H}(\rho_1, \rho_2, \Delta\rho, d) = & -\frac{1}{\rho_1} \frac{\partial}{\partial \rho_1} \rho_1 \frac{\partial}{\partial \rho_1} - \frac{1}{\rho_2} \frac{\partial}{\partial \rho_2} \rho_2 \frac{\partial}{\partial \rho_2} \\ & + V_c(\sqrt{\rho_1^2 + d^2}) + V_c(\sqrt{\rho_2^2 + d^2}) + V_c(\sqrt{(\rho_1 - \Delta\rho)^2 + d^2}) + V_c(\sqrt{(\rho_2 + \Delta\rho)^2 + d^2}) \\ & + 2 \begin{cases} V_{\text{KR}}(|\sigma(\rho_1 - \rho_2)/\lambda + \Delta\rho|) \longrightarrow X^+ \\ V_{\text{KR}}(|(\rho_1 - \rho_2)/\lambda - \Delta\rho|) \longrightarrow X^- \end{cases}. \end{aligned} \quad (1)$$

The "atomic units" are used with distance and energy measured in the units of exciton Bohr radius $a_B^* = 0.529 \text{ \AA} \varepsilon/\mu$ and Rydberg energy $Ry^* = \hbar^2/(2\mu m_0 a_B^{*2}) = e^2/(2\varepsilon a_B^*) = 13.6 \text{ eV } \mu/\varepsilon^2$,

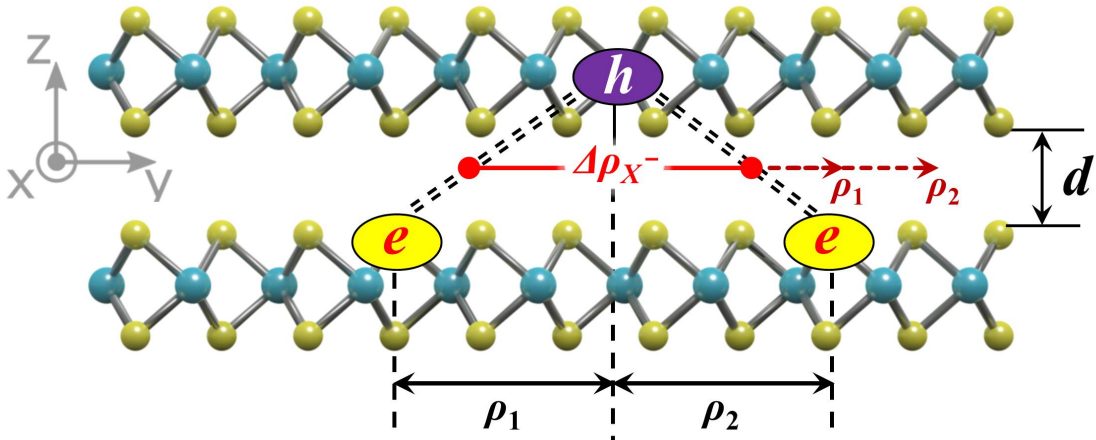


FIG. 1. The structure of a negatively charged interlayer exciton (trion) in a TMD bilayer.

respectively [3–6], $\mu = m_e/(\lambda m_0)$ with $\lambda = 1 + \sigma$ stands for the exciton reduced effective mass (in the units of free electron mass m_0), $\sigma = m_e/m_h$ is the electron-to-hole effective mass ratio, and ε represents the *effective* average dielectric constant of the entire bilayer structure [6]. The image-charge effects are neglected.

The first two lines in Eq. (1) describe the kinetic and potential energy, respectively, for the two non-interacting IEs. Their individual e - h attractive Coulomb potentials, generically of the form

$$V_c(r) = -\frac{1}{r} = -\frac{1}{\sqrt{\rho^2 + d^2}} \quad (2)$$

with ρ being the in-plane intercharge distance, are symmetrized to account for the presence of the neighbor a distance $\Delta\rho$ away as seen from the ρ_1 - and ρ_2 -coordinate systems placed at the respective IE centers of mass and treated independently (see Fig. 1). The last line is the interexciton exchange Coulomb interaction (or the like-charge Coulomb repulsion potential inside the trion) — h - h for the positive trion (X^+) and e - e for the negative trion (X^-), respectively. We use the repulsive Keldysh-Rytova (KR) interaction potential to represent this interaction

$$V_{\text{KR}}(\rho) = \frac{\pi}{(\epsilon_1 + \epsilon_2)r_0} \left[H_0\left(\frac{\rho}{r_0}\right) - N_0\left(\frac{\rho}{r_0}\right) \right], \quad (3)$$

in order to properly take into account the screening effect for the like charges confined to the same monolayer [7, 8]. Here, N_0 and H_0 are the 0th order Neumann and Struve functions, respectively, $r_0 = 2\pi\chi_{2D}$ is the screening length with χ_{2D} being the in-plane polarizability of a 2D material [9], and $\epsilon_{1,2}$ are the dielectric permittivities of its surroundings (taken to be $\epsilon_1 = \epsilon_2 = 1$ for simplicity in what follows). To facilitate the analytical calculations below, we approximate Eq. (3) by its accurate alternative written in terms of elementary functions

$$V_{\text{eff}}(\rho) = \frac{1}{r_0} \left[\ln\left(1 + \frac{r_0}{\rho}\right) + (\ln 2 - \gamma)e^{-\rho/r_0} \right] \quad (4)$$

as discussed and proposed for atomically thin layers in Ref. [10].

As described at large in Refs. [1, 2], we start the CIE binding energy calculation procedure with the (ρ_1, ρ_2) -configuration space transformation to new coordinates as follows

$$x = \begin{cases} (\rho_2 - \rho_1 - \Delta\rho)/\sqrt{2} & \longrightarrow X^+ \\ (\rho_1 - \rho_2 - \Delta\rho)/\sqrt{2} & \longrightarrow X^- \end{cases}, \quad y = \frac{\rho_1 + \rho_2}{\sqrt{2}}. \quad (5)$$

This transformation places the origin and both axes of the new coordinate system (x, y) into the intersection of the two underbarrier tunnel channels between the non-interacting

IE potential energy minima of the Hamiltonian (1), to capture the maximal tunnel flow between the two indistinguishable IE configurations. The tunnel exchange splitting integral in Eq. (1) of the main text then takes the form

$$J_{X^\pm}(\Delta\rho) = \int_{-\Delta\rho/\sqrt{2}}^{\Delta\rho/\sqrt{2}} dy \left| \psi_{X^\pm}(x, y) \frac{\partial \psi_{X^\pm}(x, y)}{\partial x} \right|_{x=0}, \quad (6)$$

where $\psi_{X^\pm}(x, y)$ is the ground-state eigenfunction of the Schrödinger equation with the Hamiltonian (1) transformed to the (x, y) coordinates. In terms of Fig. 1, for X^- the tunnel current (6) is due to the electron position exchange relative to the hole. This corresponds to the underbarrier tunneling of the entire three-particle system between the two indistinguishable configurations defined by the minima at $\rho_1 = \rho_2 = 0$ and $\rho_1 = -\rho_2 = \Delta\rho$, respectively, of the potential energy surface of the two non-interacting IEs sharing the same hole. For X^+ the tunnel current is associated with the hole position exchange relative to the electron due to the three-particle system tunneling between the two equivalent indistinguishable configurations defined by the minima at $\rho_1 = \rho_2 = 0$ and $\rho_2 = -\rho_1 = \Delta\rho$. Such a tunnel exchange is binding the three-particle system to form a stable CIE state.

The function $\psi_{X^\pm}(x, y)$ in Eq. (6) can be found in the form

$$\psi_{X^\pm}(x, y) = \phi_{IX}(x, y) \exp[-S_{X^\pm}(x, y)], \quad (7)$$

where $\phi_{IX}(x, y) = \psi_{IX}[\rho_1(x, y), d] \psi_{IX}[\rho_2(x, y), d]$ is the wave-function of the isolated two-exciton state centered at the minimum $\rho_1 = \rho_2 = 0$ (or $x = -\Delta\rho/\sqrt{2}$, $y = 0$) of the configuration potential in the second line of Eq. (1). This is the solution to the ground-state eigenvalue problem given by the first two lines of the Hamiltonian (1) — the product of the two indirect exciton (IE) wave functions ψ_{IX} with ρ_1 and ρ_2 expressed in terms of x and y using Eq. (5). The indirect exciton eigenvalue problem was studied by Leavitt and Little previously [6]. Their results for the ground-state energy E_{IX} and the wave-function ψ_{IX} are as follows (atomic units)

$$E_{IX}(d) = \alpha^2 - \frac{4\alpha + 4\alpha^4 d^2 E_1(2\alpha d) \exp(2\alpha d)}{1 + 2\alpha d}, \quad (8)$$

where $E_1(x) = \int_x^\infty dt e^{-t}/t$ is the exponential integral, $\alpha = 2/(1 + 2\sqrt{d})$, and

$$\psi_{IX}(\rho, d) = N \exp[-\alpha(\sqrt{\rho^2 + d^2} - d)], \quad (9)$$

with the normalization constant $N = 4/\sqrt{1 + 4\sqrt{d} + 8d(1 + \sqrt{d})}$ determined by

$$\int_0^\infty d\rho \rho |\psi_{IX}(\rho, d)|^2 = 1.$$

The unknown function $S_{X^\pm}(x, y)$ in Eq. (7) is assumed to be smooth and *slowly* varying in the domain of interest — the square $|x|, |y| \leq \Delta\rho/\sqrt{2}$ — to account for the major deviation of ψ_{X^\pm} from ϕ_{IX} in its "tail area" ($x \sim y \sim 0$) due to the tunnel exchange coupling of the isolated two-exciton state centered at $\rho_1 = \rho_2 = 0$ ($x = -\Delta\rho/\sqrt{2}$, $y = 0$) to another (indistinguishable) state centered at $\rho_1 = -\rho_2 = \Delta\rho$ and $\rho_2 = -\rho_1 = \Delta\rho$ ($x = \Delta\rho/\sqrt{2}$, $y = 0$) for X^- and X^+ , respectively.

(a) *The Negative Trion Case*

In our three-particle X^\pm complexes, the equivalency of the two IEs sharing the same hole (or electron) implies their identity and leads to the fact of the like charge carriers having collinear spins. The Coulomb repulsion and the Pauli exclusion principle force them to avoid each other at short interexciton center-of-mass-to-center-of-mass distance $\Delta\rho < 1$, making it possible for a stable complex to only form at $\Delta\rho \gtrsim 1$. To the first non-vanishing order in small $1/\Delta\rho$, plugging Eq. (7) into the Schrödinger equation with the Hamiltonian (1) pre-transformed to the (x, y) -coordinates as specified by Eq. (5) for X^- , one then obtains

$$\frac{\partial S_{X^-}}{\partial x} \approx \frac{\Delta\rho}{\sqrt{2}(\alpha\Delta\rho - 1)} V_{\text{KR}}\left(\frac{|\sqrt{2}x - \sigma\Delta\rho|}{\lambda}\right) \quad (10)$$

with the second order derivatives of S_{X^-} neglected (a slowly varying function). This is to be solved in the domain $|x|, |y| \leq \Delta\rho/\sqrt{2}$ with the boundary condition $S_{X^-}(-\Delta\rho/\sqrt{2}, y) = 0$ to fulfill the condition $\psi_{X^\pm}(-\Delta\rho/\sqrt{2}, y) = \phi_{IX}(-\Delta\rho/\sqrt{2}, y)$ according to Eq. (7).

To find the analytical solution of the problem, we use V_{eff} of Eq. (4) instead of V_{KR} in the right-hand side of Eq. (10). The solution to fulfill the boundary condition is given by

$$S_{X^-}(x, y) = \frac{\Delta\rho}{\sqrt{2}(\alpha\Delta\rho - 1)} \int_{-\Delta\rho/\sqrt{2}}^x dt V_{\text{eff}}\left(\frac{|\sqrt{2}t - \sigma\Delta\rho|}{\lambda}\right) = \frac{\Delta\rho}{\sqrt{2}(\alpha\Delta\rho - 1)} I(x, \Delta\rho). \quad (11)$$

To calculate the integral $I(x, \Delta\rho)$ here, we first use the unit step function to write

$$V_{\text{eff}}\left(\frac{|\sqrt{2}t - \sigma\Delta\rho|}{\lambda}\right) = \theta\left(t - \frac{\sigma\Delta\rho}{\sqrt{2}}\right) V_{\text{eff}}\left(\frac{\sqrt{2}t - \sigma\Delta\rho}{\lambda}\right) + \theta\left(\frac{\sigma\Delta\rho}{\sqrt{2}} - t\right) V_{\text{eff}}\left(\frac{\sigma\Delta\rho - \sqrt{2}t}{\lambda}\right),$$

followed by the change of variable $\tau = (\sqrt{2}t - \sigma\Delta\rho)/\lambda$ to obtain

$$\begin{aligned} I(x, \Delta\rho) = & \frac{\lambda}{\sqrt{2}} \left\{ \theta\left(x - \frac{\sigma\Delta\rho}{\sqrt{2}}\right) \left[\int_{-\Delta\rho}^0 d\tau V_{\text{eff}}(-\tau) + \int_0^{(\sqrt{2}x - \sigma\Delta\rho)/\lambda} d\tau V_{\text{eff}}(\tau) \right] \right. \\ & \left. + \theta\left(\frac{\sigma\Delta\rho}{\sqrt{2}} - x\right) \int_{-\Delta\rho}^{(\sqrt{2}x - \sigma\Delta\rho)/\lambda} d\tau V_{\text{eff}}(-\tau) \right\}. \end{aligned}$$

Of three terms here, only the third is seen to provide the solution in the domain $x < \sigma\Delta\rho/\sqrt{2}$ that includes the region $x \sim 0$ of interest to us. With V_{eff} of Eq. (4), this term can be easily calculated analytically using integration by parts. One obtains

$$I(x < \sigma\Delta\rho/\sqrt{2}, \Delta\rho) = \frac{\lambda}{\sqrt{2}} \left[\ln \frac{1+p}{1+s} + \ln \left(\frac{s}{1+s} \right)^s \left(\frac{1+p}{p} \right)^p + (\ln 2 - \gamma)(e^{-s} - e^{-p}) \right]$$

with $s = (\sigma\Delta\rho - \sqrt{2}x)/\lambda r_0$ and $p = \Delta\rho/r_0$. A close inspection of this expression reveals that since $s < p$, the first summand is predominant there and the other two are negligible for all $1 < s < p$ regardless of how big s and p individually are. After dropping the negligible terms, Eq. (11) in the domain of interest takes the final form as follows

$$S_{X^-}(x, y) \approx \frac{\lambda\Delta\rho}{2(1 - \alpha\Delta\rho)} \ln \frac{1 - \sqrt{2}x/(\lambda r_0 + \sigma\Delta\rho)}{1 + \Delta\rho/(\lambda r_0 + \sigma\Delta\rho)}, \quad (12)$$

(b) The Positive Trion Case

Under the same assumptions, plugging Eq. (7) into the Schrödinger equation with Hamiltonian (1) pre-transformed to the (x, y) -coordinates as directed by Eq. (5) for X^+ , gives

$$\frac{\partial S_{X^+}}{\partial x} \approx \frac{\Delta\rho}{\sqrt{2}(\alpha\Delta\rho - 1)} V_{\text{KR}} \left(\frac{|\sqrt{2}\sigma x - \Delta\rho|}{\lambda} \right). \quad (13)$$

It is easy to see that this equation can be obtained from Eq. (10) by the simple replacement $1/\lambda \leftrightarrow \sigma/\lambda$. Its solution in the domain of interest can then be obtained by applying this replacement to Eq. (12). This gives

$$S_{X^+}(x, y) \approx \frac{\lambda\Delta\rho}{2\sigma(1 - \alpha\Delta\rho)} \ln \frac{1 - \sqrt{2}\sigma x/(\lambda r_0 + \Delta\rho)}{1 + \sigma\Delta\rho/(\lambda r_0 + \Delta\rho)}. \quad (14)$$

(c) The Tunnel Exchange Coupling Integral

It is noteworthy that both Eq. (12) and Eq. (14) are fully consistent with the result reported for $\sigma = 1$ previously [2]. The functions ψ_{X^\pm} one obtains by plugging these equations into Eq. (7) can be used to evaluate the tunnel exchange coupling integrals J_{X^\pm} in Eq. (6). The differentiation therein can be conveniently done using the following easy-to-prove rule:

$$\text{if } F(x, y) = F_0(x, y)e^{-A(x, y)} \text{ with } F_0(x, y) = Ce^{-\gamma B(x, y)}, \text{ then}$$

$$F \frac{\partial F}{\partial(x, y)} = - \left[\frac{\partial A}{\partial(x, y)} + \gamma \frac{\partial B}{\partial(x, y)} \right] F^2 \text{ and } -\gamma \frac{\partial B}{\partial(x, y)} = \frac{1}{F_0} \frac{\partial F_0}{\partial(x, y)}.$$

Here $\partial/\partial(x, y)$ stands for either $\partial/\partial x$ or $\partial/\partial y$. With this, after simplifications and elementary integration over y one obtains $J_{X^\pm}(\Delta\rho)$ in the form of Eq. (2) in the main text.

Seeking the extremum for $J_{X^\pm}(\Delta\rho)$ must only include the leading term in small $1/\Delta\rho$ to be consistent with the procedure of finding S_{X^\pm} described above. Taking the derivative of J_{X^\pm} over $\Delta\rho$, equating it to zero, and solving the polynomial equation obtained to the first infinitesimal order in $1/\Delta\rho$, results in $\Delta\rho_{X^\pm}$ in the form of Eq. (4) in the main text.

II. THE PAIRWISE INTERACTION POTENTIALS FOR CHARGED INTERLAYER EXCITONS

As can be seen from the two special cases shown in Fig. 2 (a) and (b), the long-range Coulomb interaction of the pair of CIEs (trions) depends on the relative orientation of the triangles formed by the three charges in a trion complex. The exact interaction potential includes nine terms to couple the electrons and holes in the two spatially separated complexes.

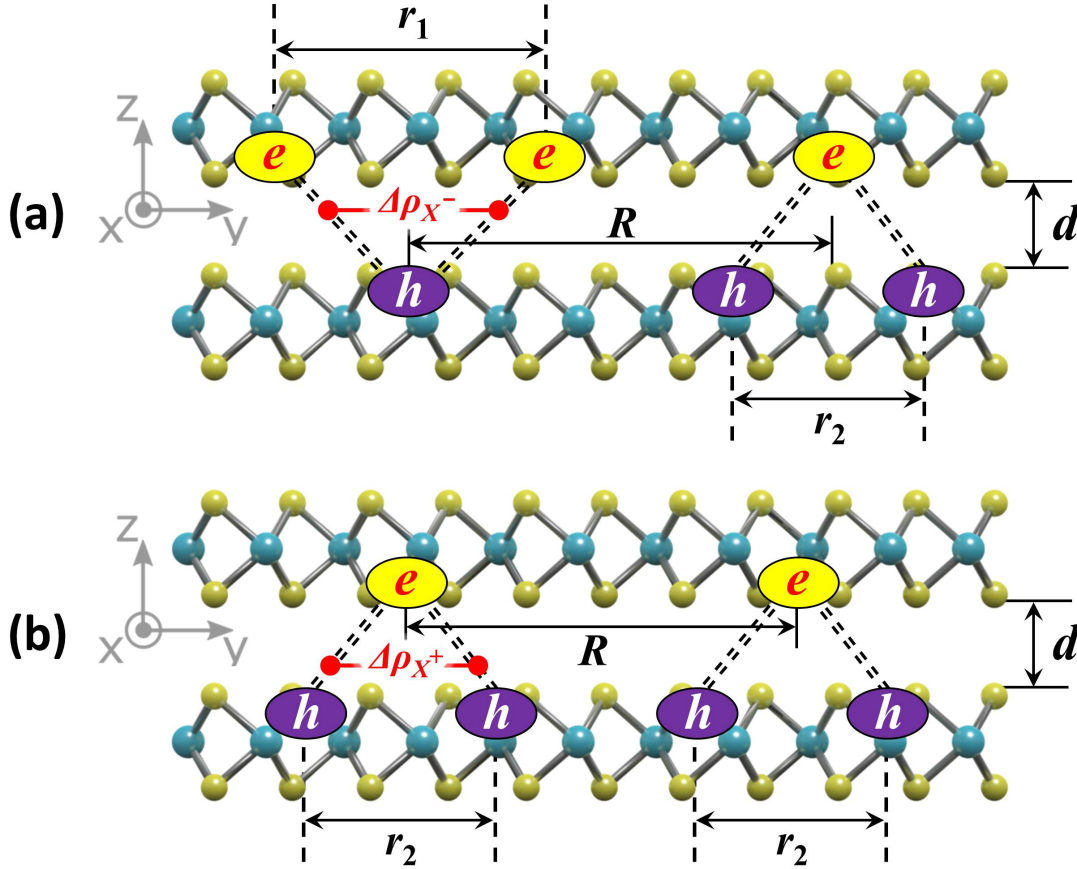


FIG. 2. The coplanar pairwise interaction geometry for the unlike-charge (a) and like-charge (b) IE complexes (trions) in a TMD bilayer.

To simulate the actual potential energy surfaces we use the Coulomb interaction coupling of Eq. (2) for the (unlike) charges located in the distinct monolayers and the KR interaction coupling of Eq. (3) for the (like) charges confined to the same monolayer. The explicit coupling parameter dependence is given by the functions $V_{\text{KR}}(R, r_1, r_2, r_0)$ and $V_{\text{C}}(R, r_1, r_2, d)$ specified below, where R is the trion-trion center-of-mass-to-center-of-mass distance and $r_{1,2}$ are the distances between the like charges in the first and second trion of the interacting trion pair. In general, $r_1 \neq r_2$ for the unlike-charge trion-trion coupling and $r_1 = r_2$ for the like-charge trion-trion coupling as sketched in Fig. 2 (a) and (b). Using the standard triangle similarity theorems, these distances come out as $\lambda\Delta\rho_{X^+}$ and $(\lambda/\sigma)\Delta\rho_{X^-}$ for the positive and negative trion, respectively. This is why for unlike-charge trion pairs, r_1 can only be equal to r_2 if $\sigma = 1$ (or $m_e = m_h$).

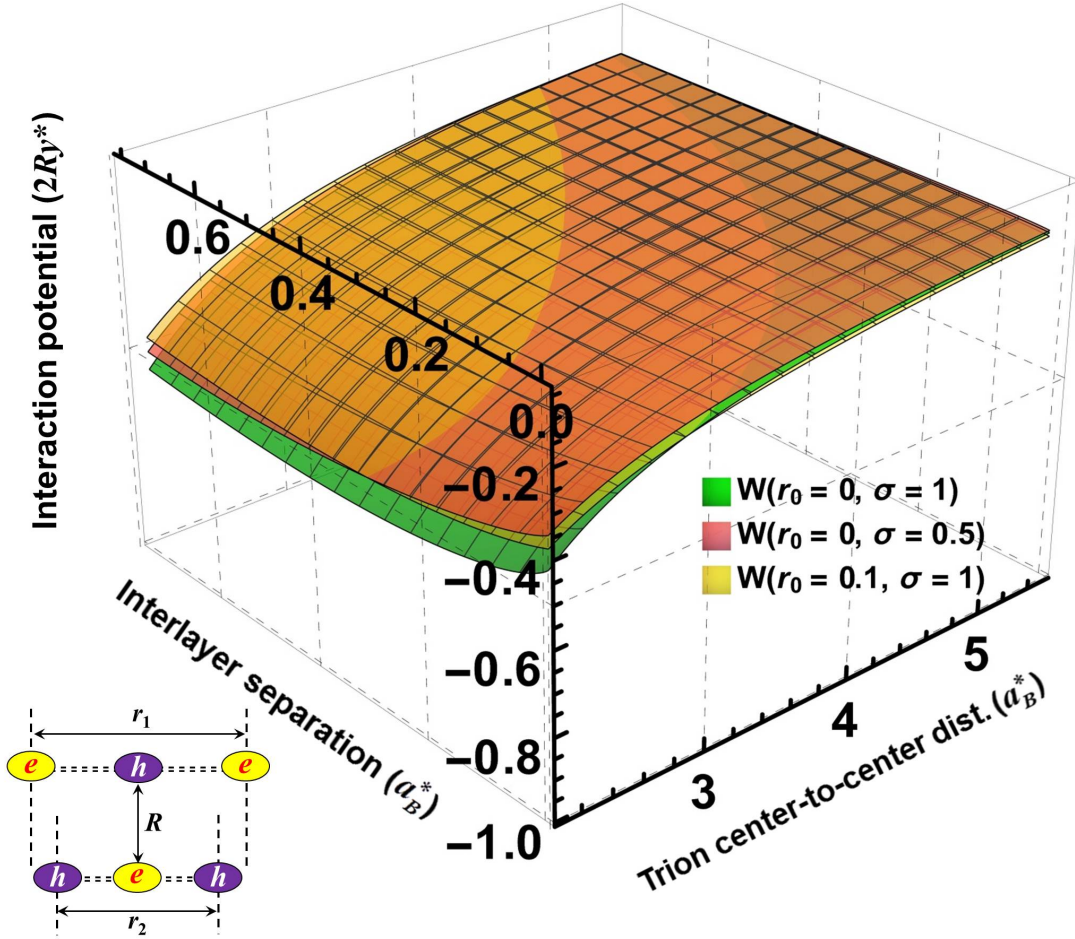


FIG. 3. The pairwise interaction potential energy W as given by Eq. (16) for the two unlike-charge IEs in the parallel biplanar relative orientation sketched at bottom left (top view).

(a) The Pairwise Interaction Potentials for Unlike-Charge IEs

In this case, two most likely relative orientations are supported by symmetry for a pair of triangle-shaped complexes in bilayer structures we deal with. They are the coplanar and parallel biplanar orientation. Their side and top views are shown in Fig. 2 (a) and in the bottom-left inset of Fig. 3, respectively. For the former, counting e - h couplings in Fig. 2 (a) counterclockwise from top left, the total interaction potential energy U takes the form

$$U = u_1 + u_2 + u_3, \quad (15)$$

$$\begin{aligned} u_1 &= V_{\text{KR}}(R + r_1/2) + V_{\text{C}}\left\{\sqrt{[R + (r_1 - r_2)/2]^2 + d^2}\right\} + V_{\text{C}}\left\{\sqrt{[R + (r_1 + r_2)/2]^2 + d^2}\right\}, \\ u_2 &= V_{\text{KR}}(R - r_2/2) + V_{\text{KR}}(R + r_2/2) + V_{\text{C}}\left(\sqrt{R^2 + d^2}\right), \\ u_3 &= V_{\text{KR}}(R - r_1/2) + V_{\text{C}}\left\{\sqrt{[R - (r_1 + r_2)/2]^2 + d^2}\right\} + V_{\text{C}}\left\{\sqrt{[R - (r_1 - r_2)/2]^2 + d^2}\right\}. \end{aligned}$$

For the latter, from the inset in Fig. 3 the total interaction potential W comes out as

$$W = 2w_1 + w_2, \quad (16)$$

$$\begin{aligned} w_1 &= V_{\text{C}}\left[\sqrt{(r_1 - r_2)^2/4 + R^2 + d^2}\right] + V_{\text{KR}}\left(\sqrt{r_1^2/4 + R^2}\right) + V_{\text{C}}\left[\sqrt{(r_1 + r_2)^2/4 + R^2 + d^2}\right], \\ w_2 &= 2V_{\text{KR}}\left(\sqrt{r_2^2/4 + R^2}\right) + V_{\text{C}}\left(\sqrt{R^2 + d^2}\right). \end{aligned}$$

The calculated interaction potentials U and W are presented in Fig. 3 (a) of the main text and in Fig. 3 herewith, respectively. The former is seen to be over an order of magnitude more attractive than the latter in the same parameter range, which is why the W interaction potential energy is neglected in the analysis we report about in the main text.

(b) The Pairwise Interaction Potentials for Like-Charge IEs

In this case, both coplanar and parallel biplanar relative orientations of the triangle-shaped complexes are strongly repulsive and, in general, are different for positively and negatively charged trion pairs. The side view of the coplanar orientation of two positive trions is shown in Fig. 2 (b). The top view of their parallel biplanar orientation can be obtained from the sketch in Fig. 3 by setting $r_1 = r_2$ and relabeling $e \leftrightarrow h$ in one of the trions. For the former, counting e - h couplings in Fig. 2 (b) counterclockwise from top left, the total interaction potential energy V takes the form

$$V = v_1 + v_2 + v_3, \quad (17)$$

$$\begin{aligned}
v_1 &= V_{\text{KR}}(R) + V_{\text{C}} \left[\sqrt{(R - r_2/2)^2 + d^2} \right] + V_{\text{C}} \left[\sqrt{(R + r_2/2)^2 + d^2} \right], \\
v_2 &= V_{\text{KR}}(R) + V_{\text{KR}}(R + r_2) + V_{\text{C}} \left[\sqrt{(R + r_2/2)^2 + d^2} \right], \\
v_3 &= V_{\text{KR}}(R - r_2) + V_{\text{KR}}(R) + V_{\text{C}} \left[\sqrt{(R - r_2/2)^2 + d^2} \right].
\end{aligned}$$

For the latter, the total interaction potential energy \bar{V} can be obtained from Eq. (16) by setting $r_1 = r_2$ and simultaneously swapping $V_{\text{KR}} \leftrightarrow V_{\text{C}}$ and $R^2 \leftrightarrow R^2 + d^2$. This gives

$$\bar{V} = 2\bar{v}_1 + \bar{v}_2, \quad (18)$$

$$\begin{aligned}
\bar{v}_1 &= V_{\text{KR}}(R) + V_{\text{C}} \left(\sqrt{r_2^2/4 + R^2 + d^2} \right) + V_{\text{KR}} \left(\sqrt{r_2^2 + R^2} \right), \\
\bar{v}_2 &= 2V_{\text{C}} \left(\sqrt{r_2^2/4 + R^2 + d^2} \right) + V_{\text{KR}}(R).
\end{aligned}$$

For a negatively charged trion pair, r_2 should be replaced with r_1 in both of these equations.

A close inspection of Eqs. (17) and (18) reveals their very similar repulsive behavior and in fact their coincidence when R is greatly different from r_2 (both greater and less than). The calculated interaction potential V of Eq. (17) is presented in Fig. 3 (a) of the main text.

III. LIKE-CHARGE TRION WIGNER CRYSTALLIZATION PARAMETERS

An ensemble of repulsively interacting particles (or quasiparticles, structureless or composite) forms a Wigner lattice when its average potential interaction energy exceeds average kinetic energy, $\langle V \rangle / \langle K \rangle = \Gamma_0 > 1$ (see, e.g., Ref. [11]). For like-charge trions in Fig. 2 (b), the Coulomb repulsion at large R ($\gg r_2$) is strengthened at shorter R by the dipole-dipole repulsion of their collinear permanent dipole moments directed perpendicular to the heterostructure plane. These are the two major terms of the power series expansion in r_2/R (< 1) of the repulsive pairwise interaction potential V presented in Fig. 3 (a) of the main text. With rotational kinetic energy neglected for the reasons explained in the main text, the like-charge trion critical density n_{cX^\pm} and temperature $T_{cX^\pm}^{(w)}$ can be obtained by drawing an analogy to the 2D electron gas system [11] to include the extra dipole-dipole repulsion term.

(a) The Critical Density

With the commonly used notations preserved, we go on with using the atomic units introduced previously. For trion-trion separation distances R greater than the size of the

trion ($R \gg r_{1,2}$), the first order power series expansion of the average repulsive trion-trion interaction potential takes the form

$$\langle V \rangle = \frac{1}{R} \left(1 + \frac{d^2}{R^2} \right) = \sqrt{\pi n} (1 + d^2 \pi n), \quad (19)$$

where $n = 1/\pi R^2$ is the trion surface density. Our trions are composite fermions with the occupation number

$$n_{\mathbf{k}} = \frac{1}{e^{\beta(E_{\mathbf{k}} - \bar{\mu})} + 1}, \quad (20)$$

where $\beta = 1/k_B T$, $E_{\mathbf{k}} = \hbar^2 k^2 / 2M$, $M = M_{X\pm}$ and $\bar{\mu}$ being the trion total mass and chemical potential, respectively. At zero T this turns into a unit-step function to give n in Eq. (19) in the form

$$n = \frac{\langle N \rangle}{S} = \frac{2}{S} \sum_{\mathbf{k}} n_{\mathbf{k}} = \frac{2}{S} \frac{S}{(2\pi)^2} 2\pi \int_0^{k_F} dk k = \frac{k_F^2}{2\pi}, \quad (21)$$

where S is the surface area and k_F is the trion Fermi-momentum. The average kinetic energy per particle can then be written as

$$\langle K \rangle = \frac{2}{\langle N \rangle} \sum_{\mathbf{k}} E_{\mathbf{k}} n_{\mathbf{k}} = \frac{2}{\langle N \rangle} \frac{S}{(2\pi)^2} 2\pi \int_0^{k_F} dk k \frac{\hbar^2 k^2}{2M} = \frac{\pi S}{\langle N \rangle} \frac{\hbar^2}{2M} \left(\frac{k_F^2}{2\pi} \right)^2 = \frac{\hbar^2}{2M} \pi n \quad (22)$$

to result, with $\langle V \rangle$ of Eq. (19), in

$$\Gamma_0 = \frac{\langle V \rangle}{\langle K \rangle} = \frac{2M}{\hbar^2} \frac{1 + d^2 \pi n}{\sqrt{\pi n}} = \frac{2}{g} \frac{1 + d^2 \pi n}{\sqrt{\pi n}}, \quad (23)$$

where g stands for the ratio of the electron-hole reduced mass to the trion total mass

$$g = \frac{\mu}{M} = \frac{\mu}{M_{X\pm}} = g_{\pm}(\sigma) = \left(3 + \left\{ \frac{1}{2} \right\} \sigma + \left\{ \frac{2}{1} \right\} \frac{1}{\sigma} \right)^{-1}. \quad (24)$$

Introducing the new variable $t = d\sqrt{\pi n}$ turns Eq. (23) into a quadratic equation

$$t^2 - \frac{g\Gamma_0}{2d} t + 1 = 0$$

with two roots as follows

$$t_{1,2} = \frac{g\Gamma_0}{4d} \pm \sqrt{\left(\frac{g\Gamma_0}{4d} \right)^2 - 1},$$

of which only one, t_2 , stays finite as d goes down to zero. This root leads to

$$n_{cX\pm} = \frac{2}{\pi d^2} \left(\frac{g_{\pm}\Gamma_0}{4d} \right)^2 \left[1 - \frac{1}{2} \left(\frac{4d}{g_{\pm}\Gamma_0} \right)^2 - \sqrt{1 - \left(\frac{4d}{g_{\pm}\Gamma_0} \right)^2} \right] \quad (25)$$

and reproduces the result of Ref. [11] for $d \rightarrow 0$ and $g_{\pm} = 1$.

(b) *The Critical Temperature*

For arbitrary nonzero T , using Eq. (20) with the new variable $x = \hbar k \sqrt{\beta/2M}$, the trion surface density (21) can be written in a parametric form as follows

$$n = \frac{\langle N \rangle}{S} = \frac{2}{S} \frac{S}{(2\pi)^2} 2\pi \int_0^\infty \frac{dk k}{e^{\beta(E_{\mathbf{k}} - \bar{\mu})} + 1} = \frac{2M}{\hbar^2 \pi \beta} \int_0^\infty dx x \frac{ze^{-x^2}}{1 + ze^{-x^2}}, \quad z = e^{\beta \bar{\mu}} \geq 0. \quad (26)$$

Similarly, the average kinetic energy per particle of Eq. (22) takes the form

$$\langle K \rangle = \frac{2}{\langle N \rangle} \frac{S}{(2\pi)^2} 2\pi \frac{\hbar^2}{2M} \int_0^\infty \frac{dk k^3}{e^{\beta(E_{\mathbf{k}} - \bar{\mu})} + 1} = \frac{1}{\beta} \frac{\int_0^\infty dx x^3 \frac{ze^{-x^2}}{1 + ze^{-x^2}}}{\int_0^\infty dx x \frac{ze^{-x^2}}{1 + ze^{-x^2}}}. \quad (27)$$

After the power series expansions of their respective denominators, these integrals can further be represented in terms of the gamma and polylogarithm functions following the rule

$$\sum_{m=1}^\infty \int_0^\infty x^n (-ze^{-x^2})^m dx = \frac{\Gamma[(n+1)/2]}{2} \text{Li}_{(n+1)/2}(-z) = \frac{\Gamma[(n+1)/2]}{2} \sum_{m=1}^\infty \frac{(-z)^m}{m^{(n+1)/2}}. \quad (28)$$

In the classical limit (high T and/or low density; see, e.g., Ref. [12]), one has $e^{\beta(E_{\mathbf{k}} - \bar{\mu})} \gg 1$, so that the occupation number (20) takes the form $n_{\mathbf{k}} = e^{-\beta(E_{\mathbf{k}} - \mu)} = ze^{-\beta E_{\mathbf{k}}}$ to simplify n in Eq. (26) as follows

$$n = \frac{2Mz}{\hbar^2 \pi \beta} \int_0^\infty dx x e^{-x^2} = \frac{Mz}{\hbar^2 \pi \beta}, \quad (29)$$

whereby the kinetic energy per particle of Eq. (27) takes the form

$$\langle K \rangle = \frac{2Mz}{\hbar^2 \pi \beta^2 n} \int_0^\infty dx x^3 e^{-x^2} = \frac{Mz}{\hbar^2 \pi \beta^2 n} = \frac{1}{\beta} = k_B T \quad (30)$$

as expected from the energy equipartition theorem of classical statistical mechanics.

Plugging Eqs. (19) and (30) in Eq. (23) gives the equality $\pi n(1 + d^2 \pi n)^2 = (\Gamma_0 k_B T)^2$. In this equation, to make it consistent with the approximation Eq. (19) is valid within, one has to discard the terms with powers of d higher than d^2 . The quadratic equation thus obtained gives two roots for $n(T)$, one of which is manifestly negative and so to be discarded. Equating the other root to n_{cX^\pm} of Eq. (25) gives the constraint for the critical temperature. Solving it for T subject to keeping powers of d no greater than d^2 , leads to

$$k_B T_{cX^\pm}^{(w)} = \frac{4}{g_\pm \Gamma_0^2}$$

(in the units of Ry^*) with $g_\pm(\sigma)$ given by Eq. (24). This agrees with Ref. [11] for $g_\pm = 1$.

-
- [1] I.V.Bondarev, Configuration space method for calculating binding energies of exciton complexes in quasi-1D/2D semiconductors, *Mod. Phys. Lett. B* **30**, 1630006 (2016).
- [2] I.V.Bondarev and M.R.Vladimirova, Complexes of dipolar excitons in layered quasi-two-dimensional nanostructures, *Phys. Rev. B* **97**, 165419 (2018).
- [3] L.D.Landau and E.M.Lifshitz, *Quantum Mechanics. Non-Relativistic Theory* (Pergamon, Oxford, 1991).
- [4] L.P.Gor'kov and L.P.Pitaevski, The splitting energy of hydrogen molecule terms, *Dokl. Akad. Nauk SSSR* **151**, 822 (1963) [English transl.: *Soviet Phys.—Dokl.* **8**, 788 (1964)].
- [5] C.Herring, Critique of the Heitler-London method of calculating spin couplings at large distances, *Rev. Mod. Phys.* **34**, 631 (1962); C.Herring and M.Flicker, Asymptotic exchange coupling of two hydrogen atoms, *Phys. Rev.* **134**, A362 (1964).
- [6] R.P.Leavitt and J.W.Little, Simple method for calculating exciton binding energies in quantum-confined semiconductor structures, *Phys. Rev. B* **42**, 11774 (1990).
- [7] L.V.Keldysh, Coulomb interaction in thin semiconductor and semimetal films, *Sov. Phys. JETP* **29**, 658 (1979).
- [8] N.S.Rytova, Screened potential of a point charge in a thin film, *Proc. MSU Phys., Astron.* **3**, 30 (1967).
- [9] T.C.Berkelbach, M.S.Hybertsen, and D.R.Reichman, Theory of neutral and charged excitons in monolayer transition metal dichalcogenides, *Phys. Rev. B* **88**, 045318 (2013).
- [10] P.Cudazzo, I.V.Tokatly, and A.Rubio, Dielectric screening in two-dimensional insulators: Implications for excitonic and impurity states in graphene, *Phys. Rev. B* **84**, 085406 (2011).
- [11] P.M.Platzman and H.Fukuyama, Phase diagram of the two-dimensional electron liquid, *Phys. Rev. B* **10**, 3150 (1974).
- [12] D.Chandler, *Introduction to Modern Statistical Mechanics*, (Oxford University Press, New York, 1987), p. 101.